



## Thermal Stability of Volatiles in the North Polar Region of Mercury

David A. Paige *et al.*  
*Science* **339**, 300 (2013);  
DOI: 10.1126/science.1231106

*This copy is for your personal, non-commercial use only.*

If you wish to distribute this article to others, you can order high-quality copies for your colleagues, clients, or customers by [clicking here](#).

Permission to republish or repurpose articles or portions of articles can be obtained by following the guidelines [here](#).

**The following resources related to this article are available online at [www.sciencemag.org](http://www.sciencemag.org) (this information is current as of July 24, 2013):**

**Updated information and services**, including high-resolution figures, can be found in the online version of this article at:

<http://www.sciencemag.org/content/339/6117/300.full.html>

**Supporting Online Material** can be found at:

<http://www.sciencemag.org/content/suppl/2012/11/28/science.1231106.DC1.html>

A list of selected additional articles on the Science Web sites **related to this article** can be found at:

<http://www.sciencemag.org/content/339/6117/300.full.html#related>

This article **cites 48 articles**, 8 of which can be accessed free:

<http://www.sciencemag.org/content/339/6117/300.full.html#ref-list-1>

This article has been **cited by 4 articles** hosted by HighWire Press; see:

<http://www.sciencemag.org/content/339/6117/300.full.html#related-urls>

This article appears in the following **subject collections**:

Planetary Science

[http://www.sciencemag.org/cgi/collection/planet\\_sci](http://www.sciencemag.org/cgi/collection/planet_sci)

- many craters are not resolved by MLA, we also selected craters with diameters  $\geq 7$  km from MESSENGER images. Smaller RB deposits were not considered because most appear from images to lie in small secondary craters, at the foot of poleward-facing scarps, or in rough terrain and are inadequately sampled by MLA. The radar-bright deposits were mapped with a threshold of 0.075 in the MATLAB image processing toolbox and correlated with craters identified in MLA topography and MESSENGER images. Labels assigned in uppercase are consistent with previous nomenclature (15); lowercase letters and numerals were assigned to provisional features. Regions with MLA energy measurements were classified as dark, normal, or bright/mixed according to their contrast in brightness with those of surround areas; gaps in high-threshold returns were also taken to indicate darker material. Bright regions are surrounding those for which more than half of the returns have  $r_s > 0.3$ .
23. Diameters of large craters were fit to the maximum MLA topographic contours of the rims, whereas the diameters of smaller craters were estimated from Mercury Dual Imaging System (34) image mosaics. Locations are less certain for smaller features inadequately sampled by MLA. Diameters of craters sampled ranged from 7 to 108 km, not including the 320-km-diameter Goethe basin. Not included are several degraded and partially flooded craters, such as a 133-km-diameter degraded crater that encloses Purcell but for which the relief does not create an area of permanent shadow.
  24. D. A. Paige, S. E. Wood, A. R. Vasavada, *Science* **258**, 643 (1992).
  25. D. A. Paige *et al.*, *Science* **339**, 300 (2013); 10.1126/science.1231106.
  26. D. J. Lawrence *et al.*, *Science* **339**, 292 (2013); 10.1126/science.1229953.
  27. B. J. Butler, *J. Geophys. Res.* **102**, 19,283 (1997).
  28. J. A. Zhang, D. A. Paige, *Geophys. Res. Lett.* **36**, L16203 (2009).
  29. J. A. Zhang, D. A. Paige, *Geophys. Res. Lett.* **37**, L03203 (2010).
  30. T. B. McCord, J. B. Adams, *Science* **178**, 745 (1972).
  31. F. Vilas, *Icarus* **64**, 133 (1985).

32. W. E. McClintock *et al.*, *Science* **321**, 62 (2008).
33. T. Gehrels, *Astrophys. J.* **123**, 331 (1956).
34. S. E. Hawkins III *et al.*, *Space Sci. Rev.* **131**, 247 (2007).

**Acknowledgments:** The MESSENGER project is supported by the NASA Discovery Program under contracts NAS5-97271 to the Johns Hopkins University Applied Physics Laboratory and NASW-00002 to the Carnegie Institution of Washington. We are grateful for the myriad of contributions from the MLA instrument and MESSENGER spacecraft teams and for comments by P. Lucey and two anonymous referees that improved the manuscript.

#### Supplementary Material

www.sciencemag.org/cgi/content/full/science.1229764/DC1  
Supplementary Text  
Figs. S1 to S5  
Reference (35)

5 September 2012; accepted 14 November 2012  
Published online 29 November 2012;  
10.1126/science.1229764

## Thermal Stability of Volatiles in the North Polar Region of Mercury

David A. Paige,<sup>1\*</sup> Matthew A. Siegler,<sup>1,2</sup> John K. Harmon,<sup>3</sup> Gregory A. Neumann,<sup>4</sup> Erwan M. Mazarico,<sup>4</sup> David E. Smith,<sup>5</sup> Maria T. Zuber,<sup>5</sup> Ellen Harju,<sup>1</sup> Mona L. Delitsky,<sup>6</sup> Sean C. Solomon<sup>7,8</sup>

Thermal models for the north polar region of Mercury, calculated from topographic measurements made by the MErcury Surface, Space ENvironment, GEOchemistry, and Ranging (MESSENGER) spacecraft, show that the spatial distribution of regions of high radar backscatter is well matched by the predicted distribution of thermally stable water ice. MESSENGER measurements of near-infrared surface reflectance indicate bright surfaces in the coldest areas where water ice is predicted to be stable at the surface, and dark surfaces within and surrounding warmer areas where water ice is predicted to be stable only in the near subsurface. We propose that the dark surface layer is a sublimation lag deposit that may be rich in impact-derived organic material.

Earth-based radar observations have yielded maps of anomalously bright, depolarizing features on Mercury that appear to be localized in permanently shadowed regions near the planet's poles (1, 2). Observations of similar radar signatures over a range of radar wavelengths imply that the radar-bright features correspond to deposits that are highly transparent at radar wavelengths and extend to depths of several meters below the surface (3). Cold-trapped water ice has been proposed as the most likely material to be responsible for these features (2, 4, 5), but other volatile species that are abundant on Mercury, such as sulfur, have also been suggested (6).

Measurements of surface reflectance at a wavelength of 1064 nm, made with the Mercury Laser Altimeter (MLA) onboard the MESSENGER (MErcury Surface, Space ENvironment, GEOchemistry, and Ranging) spacecraft, have revealed the presence of surface material that collocates approximately with radar-bright areas within north polar craters and that has approximately half the average reflectance of the planet, as well as bright material within Kandinsky and Prokofiev craters that has approximately twice the average planetary reflectance (7). MLA measurements have also provided detailed maps of the topography of Mercury's north polar region (8). Here, we apply this information in conjunction with a ray-tracing thermal model, previously used to predict temperatures in the polar regions of Earth's Moon (9), to calculate the thermal stability of volatile species in the north polar region of Mercury.

Maximum and average modeled temperatures (10) over one complete 2-year illumination cycle for the north polar region of Mercury are shown in Fig. 1, A and B. The topography model north of 84°N latitude has been extrapolated from only a few off-nadir data tracks, so model temperatures within this circle should be taken only as

estimates. On Mercury, biannual average temperatures can be interpreted as close approximations to the nearly constant subsurface temperatures that exist below the penetration depths of the diurnal temperature wave [about 0.3 to 0.5 m for ice-free regolith, and several meters for ice-rich areas (5, 9)]. The latitudinal and longitudinal symmetries in surface and near-surface temperatures result from Mercury's near-zero obliquity, eccentric orbit, and 3:2 spin-orbit resonance (11, 12).

Comparison between the areal coverage of model-calculated biannual maximum and average temperatures and the thermal stability of a range of candidate volatile species (Fig. 2) provides strong evidence that Mercury's anomalous radar features are due dominantly to the presence of thermally stable water ice, rather than some other candidate frozen volatile species. Within the region sampled, the vast majority of locations within which biannual average temperatures are less than ~100 K are radar-bright, whereas for areas with biannual average temperatures of greater than 100 K there are almost no radar-bright deposits (Fig. 2C). This distribution suggests that the radar-bright features are due to the presence of a volatile species that is not thermally stable at temperatures higher than ~100 K. Because of the exponential dependence of vacuum sublimation loss rates with temperature, the thermal stabilities of the candidate volatile species shown in Fig. 2A over time scales of millions to billions of years are well separated in temperature. As shown in Fig. 2A and fig. S8, 1 mm of exposed water ice—or 1 mm of water ice buried beneath a 10-cm-thick lag deposit—would sublimate to a vacuum in 1 billion years at temperatures of 100 to 115 K, which we interpret as strong evidence that Mercury's anomalous radar features are due dominantly to the presence of thermally stable water ice. If the radar-bright deposits were composed primarily of a material with a higher or lower volatility than water ice, we would expect them to be thermally stable in areas with lower or higher annual average temperatures than we observe. As illustrated in Fig. 2, B and C, the fractional areal coverage of radar-bright regions that are also just sufficiently

<sup>1</sup>Department of Earth and Space Sciences, University of California, Los Angeles, CA 90095, USA. <sup>2</sup>Jet Propulsion Laboratory, Pasadena, CA 91109, USA. <sup>3</sup>National Astronomy and Ionosphere Center, Arecibo, PR 00612, USA. <sup>4</sup>NASA Goddard Space Flight Center, Greenbelt, MD 20771, USA. <sup>5</sup>Department of Earth, Atmospheric and Planetary Sciences, Massachusetts Institute of Technology, Cambridge, MA 02139, USA. <sup>6</sup>California Specialty Engineering, Flintridge, CA 91012, USA. <sup>7</sup>Department of Terrestrial Magnetism, Carnegie Institution of Washington, Washington, DC 20015, USA. <sup>8</sup>Lamont-Doherty Earth Observatory, Columbia University, Palisades, NY 10964, USA.

\*To whom correspondence should be addressed. E-mail: dap@moon.ucla.edu

cold to trap subsurface water is nearly unity, whereas for elemental sulfur, the fractional area is less than 1 in 500. Although the temperatures of Mercury's radar-bright regions are not a good match to thermal stability temperatures of sulfur, the existence of cold traps at lower latitudes dominated by sulfur and other less volatile cold-trapped species cannot be excluded, nor can the possibility that Mercury's water-ice cold traps themselves also contain minor quantities of less volatile cold-trapped species.

The calculated depths at which near-surface water ice would be lost to sublimation at a rate of less than 1 mm per billion years, under the assumption that the ice deposits are covered by material that has the same thermophysical properties as average surface material on Mercury (5, 10), are shown in Fig. 1C. The thermal model results predict that most of Mercury's water ice deposits equatorward of 83°N would be ther-

mally stable only if buried beneath a ~10-cm-thick layer of low-conductivity, ice-free, soil-like material—a result consistent with interpretations of available radar data (3). At higher latitudes, the thermal model results predict that temperatures in larger impact craters are sufficiently cold to permit the stability of surface ice deposits. The observation of anomalously high MLA surface reflectance values in Kandinsky and Prokofiev craters (7) is consistent with the interpretation that the polar deposits in those craters contain water ice exposed at the surface.

Comparisons of the areal coverage of model-calculated biannual maximum and average temperatures for MLA-dark areas to all areas measured by MLA in the circumpolar region 75° to 83°N are shown in Fig. 2, D and E. The MLA-dark regions display a wider range of temperatures and are spatially more extensive than the radar-bright regions, even after accounting for Earth visibility.

Area ratios for biannual maximum temperatures in MLA-dark regions peak near 0.8 at ~160 K and decrease rapidly at progressively lower temperatures. We interpret this trend as indicating an increasing tendency for the thermal stability of bright surface water ice deposits as biannual maximum temperatures approach 100 K, which we document in an unusually cold impact crater at 82.0°N, 215°E (fig. S3).

In total, the results of the thermal model calculations combined with radar and MLA reflectance measurements present a quantitatively consistent case that Mercury's polar deposits are composed dominantly of water ice. This conclusion is independently reinforced by measurements of the flux of fast and epithermal neutrons made with MESSENGER's Neutron Spectrometer (13). In the region studied, radar-bright deposits are observed to be in essentially every surface and subsurface location where water ice is thermally

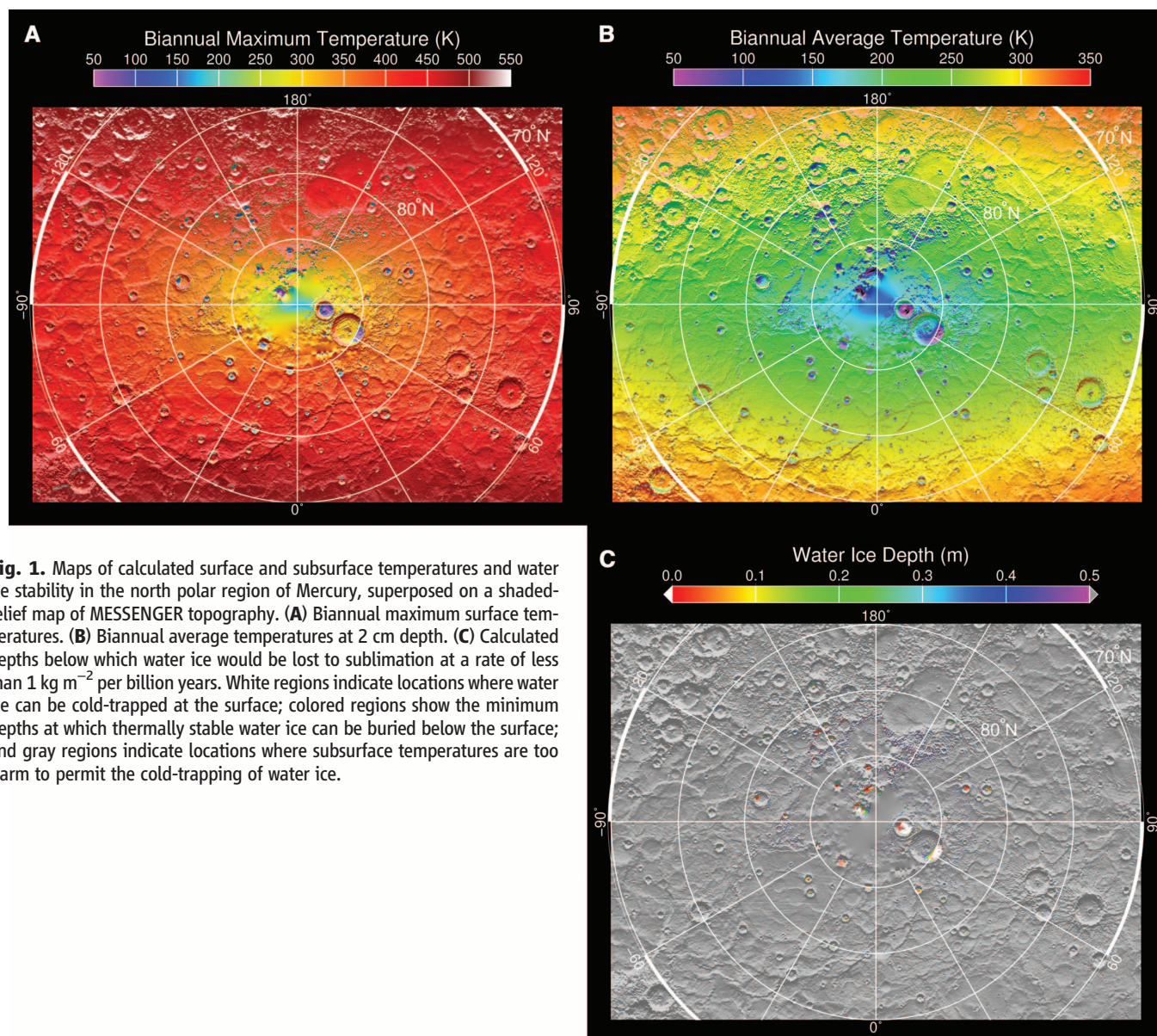


**Fig. 1.** Maps of calculated surface and subsurface temperatures and water ice stability in the north polar region of Mercury, superposed on a shaded-relief map of MESSENGER topography. **(A)** Biannual maximum surface temperatures. **(B)** Biannual average temperatures at 2 cm depth. **(C)** Calculated depths below which water ice would be lost to sublimation at a rate of less than  $1 \text{ kg m}^{-2}$  per billion years. White regions indicate locations where water ice can be cold-trapped at the surface; colored regions show the minimum depths at which thermally stable water ice can be buried below the surface; and gray regions indicate locations where subsurface temperatures are too warm to permit the cold-trapping of water ice.

stable, despite the activity of such ice destruction processes as Lyman  $\alpha$  photodissociation (14) and burial by meteoroid gardening (15). Calculated temperatures in the coldest locations on Mercury are sufficiently low that water molecules in these cold traps have very little diffusive mobility (16). The fact that bright surface ice deposits are observed in these locations requires a geologically recent or ongoing supply of water. In regions of currently stable ground ice, temperatures are sufficiently warm to allow for diffusive vertical and lateral mobility of water (17), which has enabled water to actively migrate to sites of present thermal stability.

The thermal model results provide insights into the nature and origin of MLA-dark surface deposits. Figure 2D shows that equatorward of 84°N dark material is found almost universally in regions with biannual average temperatures of 100 K and biannual maximum temperatures of 160 K, but dark material is entirely absent in regions with biannual average temperatures greater than 210 K and biannual maximum temperatures greater than 300 K. This systematic temperature dependence would not be apparent if the dark material were being redistributed about this region by impact processes alone. The distribution of dark material must be controlled by the presence of volatile substances that are not thermally stable above these temperatures. Given the clear association between the dark material and water ice that exists on Mercury today, we suggest that one of these volatile substances is water. As shown in Fig. 2A and fig. S7, the temperature at which a water ice deposit can be considered thermally stable depends on the time scale under consideration. At a temperature of 102 K, for instance, a meter-thick layer of pure water ice would sublimate to space in 1 billion years, whereas at a temperature of 210 K, a meter-thick layer of pure water ice would sublimate in 35 days.

We suggest that the MLA-dark deposits are largely sublimation lags formed on the surfaces of metastable water ice—that is, that Mercury's polar deposits were more extensive at some point in the past, and then retreated rapidly to their present long-term thermally stable state. Because Mercury's low obliquity [ $2.04 \pm 0.08$  arc min (18)] is likely to have persisted since its capture into a Cassini state  $>3.5$  billion years ago (19), thermal conditions at Mercury's poles have been relatively stable. The formation of the MLA-dark deposits by sublimation lag requires episodic, but temporally coincident, sources of both water and nonwater contaminants. Because metastable ice deposits must accumulate on time scales that are shorter than those at which they sublimate, the formation of the MLA-dark deposits by sublimation lag is compatible with episodic deposition of water and other volatiles by asteroids and comets.

The composition of the MLA-dark deposits is not known. However, materials with similarly low albedos are routinely observed on the surfaces of comets (20, 21), asteroids (22–24), and outer solar system objects (25, 26) and are generally

attributed to the presence of macromolecular carbonaceous material, rather than to the effects of radiation damage of pure ice (22, 24–26). As shown in Fig. 2, the thermal stability temperatures of a selection of simple organic compounds are such that if they were present in the Mercury polar environment, they would be readily incorporated into accumulating water ice deposits and cold-trapped directly onto surrounding warmer regions. The processing of simple organic material into dark macromolecular carbonaceous material is facilitated by high-energy photons and particles (10, 27–31), which are abundant in Mercury's polar environment because of the configuration of magnetic field lines and the pattern of ion precipitation at Mercury's high latitudes (10, 32, 33). Under this scenario, asteroidal and cometary impacts episodically release water and simple organic compounds into the Mercury en-

vironment, where they migrate to the polar regions, become cold-trapped, and accumulate. The mixture of water ice and organic material sublimates and is reprocessed to form a dark sublimation lag deposit that is analogous to that observed on the surfaces of comet nuclei today. The radar absorption properties of low-density macromolecular carbonaceous material have been measured and are found to be less lossy than low-density soil (34). Therefore, the presence of a layer of organic-rich material overlying ground ice deposits, or the presence of minor concentrations of organic-rich material within ice deposits, is not inconsistent with available radar observations. The possibility for synthesis of organic compounds in the permanently shadowed regions of Earth's Moon has been suggested (35), and the spectroscopic detection of simple organic compounds during the impact of the Lunar Crater

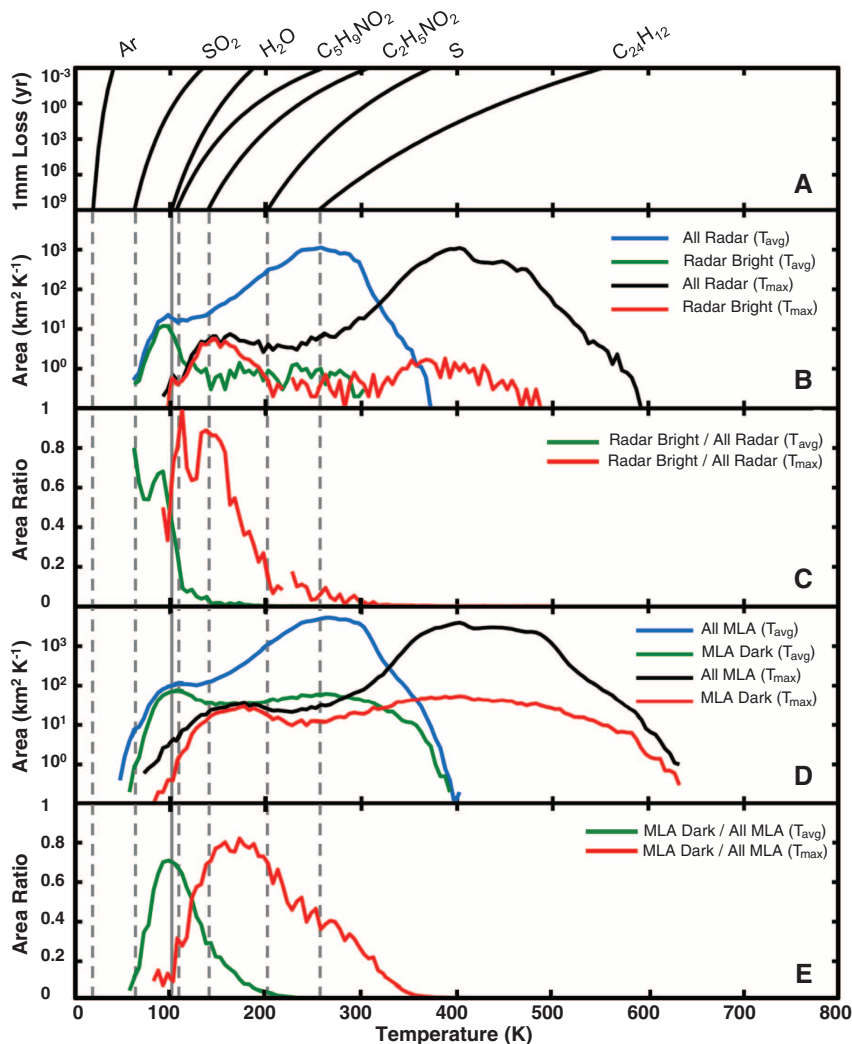


**Fig. 2.** Histograms of calculated biannual maximum ( $T_{\max}$ ) and biannual average ( $T_{\text{avg}}$ ) temperatures for radar-bright and MLA-dark areas in the north polar region of Mercury compared with the stability temperatures of a range of candidate volatile species. (A) Vacuum sublimation loss times for 1-mm-thick pure layers of selected cold-trapped volatile species as a function of temperature (37, 38). (B and C) Temperature histograms and areal coverage for radar-bright areas within Earth-visible areas at the times of the radar measurements in the region 75° to 83°N, 30° to 90°E (39). (D and E) Temperature histograms and areal coverage for MLA-dark areas for the region 75° to 83°N.

Observation and Sensing Satellite (36) provides further evidence that organic material and organic precursors coexist within the polar cold traps of solar system airless bodies.

Forming Mercury's ground ice deposits via the sublimation of a mixture of water ice and organic contaminants solves a long-standing problem regarding their origin. Today, thick deposits of ground ice are found near 75°N in areas with biannual maximum surface temperatures in excess of 150 K. At these temperatures, pure exposed water ice deposited by a cometary impact would sublimate at a rate of 1 m per 1000 years. The ice deposit would disappear on time scales of tens of thousands of years if not thermally protected by a ~10-cm-thick layer of overlying ice-free material, but this geometry is problematic because the time scales for burial to these depths by impact-gardened soil from adjacent regions is estimated to be on the order of tens of millions of years (3, 15). If Mercury's ground ice deposits contain sufficient less-volatile cold-trapped contaminants to create a surface lag deposit as they sublimate, then it would not be necessary to invoke a recent cometary impact to explain their present vertical and horizontal distribution. The fact that all of Mercury's surface and subsurface water ice deposits appear to be in a thermally stable configuration means that the sources of water and the mobility of water in Mercury's environment are sufficiently robust to overcome the combined effects of all other processes that would tend to destroy and disrupt them.

#### References and Notes

1. M. A. Slade, B. J. Butler, D. O. Muhleman, *Science* **258**, 635 (1992).
2. J. K. Harmon, M. A. Slade, M. S. Rice, *Icarus* **211**, 37 (2011).

3. J. K. Harmon, *Space Sci. Rev.* **132**, 307 (2007).
4. D. A. Paige, S. E. Wood, A. R. Vasavada, *Science* **258**, 643 (1992).
5. A. R. Vasavada, D. A. Paige, S. E. Wood, *Icarus* **141**, 179 (1999).
6. A. L. Sprague, D. M. Hunten, K. Lodders, *Icarus* **118**, 211 (1995).
7. G. A. Neumann *et al.*, *Science* **339**, 296 (2013); 10.1126/science.1229764.
8. M. T. Zuber *et al.*, *Science* **336**, 217 (2012).
9. D. A. Paige *et al.*, *Science* **330**, 479 (2010).
10. See supplementary materials on Science Online.
11. S. Soter, J. Ulrichs, *Nature* **214**, 1315 (1967).
12. Despite the extreme range of surface temperatures on Mercury, Fig. 1B indicates that there exists a ~4°-wide circumpolar zone with annual average temperatures between 273 and 373 K, a potential near-surface environment for liquid water that is the most extensive in the solar system outside Earth.
13. D. J. Lawrence *et al.*, *Science* **339**, 292 (2013); 10.1126/science.1229953.
14. T. H. Morgan, D. E. Shemansky, *J. Geophys. Res.* **96**, 1351 (1991).
15. D. Crider, R. M. Killen, *Geophys. Res. Lett.* **32**, L12201 (2005).
16. N. Schorghofer, G. J. Taylor, *J. Geophys. Res.* **112**, E02010 (2007).
17. M. A. Siegler, B. G. Bills, D. A. Paige, *J. Geophys. Res.* **116**, E03010 (2011).
18. J. L. Margot *et al.*, *J. Geophys. Res.* **117**, E00L09 (2012).
19. S. J. Peale, *Astrophys. J.* **79**, 722 (1974).
20. R. Z. Sagdeev *et al.*, *Nature* **321**, 262 (1986).
21. H. U. Keller, L. Jorda, in *The Century of Space Science*, J. A. M. Bleeker, J. Geiss, M. Huber, Eds. (Kluwer Academic, Dordrecht, Netherlands, 2001), vol. 2, pp. 1235–1276.
22. J. Gradie, J. Veverka, *Nature* **283**, 840 (1980).
23. E. F. Tedesco *et al.*, *Astron. J.* **97**, 580 (1989).
24. J. F. Bell, D. R. Davis, W. K. Hartmann, M. J. Gaffey, in *Asteroids II*, R. P. Binzel, T. Gehrels, M. S. Matthews, Eds. (Univ. of Arizona Press, Tucson, AZ, 1989), pp. 921–945.
25. D. P. Cruikshank, C. M. Dalle Ore, *Earth Moon Planets* **92**, 315 (2003).
26. D. P. Cruikshank, T. L. Roush, M. J. Bartholomew, T. R. Geballe, Y. J. Pendleton, *Icarus* **135**, 389 (1998).
27. D. L. Mitchell *et al.*, *Icarus* **98**, 125 (1992).
28. R. E. Johnson, J. F. Cooper, L. J. Lanzerotti, G. Strazzulla, *Astron. Astrophys.* **187**, 889 (1987).
29. L. J. Lanzerotti *et al.*, *J. Geophys. Res.* **92**, 14949 (1987).
30. R. E. Johnson, *J. Geophys. Res.* **96**, 17553 (1991).
31. R. E. Johnson, in *Solid-State Astrophysics, Enrico Fermi Series*, G. Strazzulla, E. Bussoletti, Eds. (North Holland, Amsterdam, 1991), pp. 129–168.
32. J. A. Slavin *et al.*, *Science* **324**, 606 (2009).
33. N. Mouawad *et al.*, *Icarus* **211**, 21 (2011).
34. P. Pailou *et al.*, *Geophys. Res. Lett.* **35**, L18202 (2008).
35. P. G. Lucey, *Proc. SPIE* **4137**, 84 (2000).
36. A. Colaprete *et al.*, *Science* **330**, 463 (2010).
37. J. A. Zhang, D. A. Paige, *Geophys. Res. Lett.* **36**, L16203 (2009).
38. J. A. Zhang, D. A. Paige, *Geophys. Res. Lett.* **37**, L03203 (2010).
39. This region was selected because it has the highest density of Earth-based radar measurements at the most favorable viewing geometries.

**Acknowledgments:** Supported by NASA grant NNX07AR64G. We thank L. Carter, A. McEwen, D. Schriver, and M. Slade for assistance with this research. The MESSENGER project is supported by the NASA Discovery Program under contract NAS5-97271 to The Johns Hopkins University Applied Physics Laboratory and NASW-00002 to the Carnegie Institution of Washington. MESSENGER data used in this study are available through the NASA Planetary Data System Geosciences Node. Arecibo radar data used in this study are available at [www.naic.edu/~radarusr/Mercpole](http://www.naic.edu/~radarusr/Mercpole).

#### Supplementary Materials

[www.sciencemag.org/cgi/content/full/science.1231106/DC1](http://www.sciencemag.org/cgi/content/full/science.1231106/DC1)  
Materials and Methods  
Figs. S1 to S8  
References (40–56)

4 October 2012; accepted 14 November 2012  
Published online 29 November 2012;  
10.1126/science.1231106

## An Efficient Polymer Molecular Sieve for Membrane Gas Separations

Mariolino Carta,<sup>1</sup> Richard Malpass-Evans,<sup>1</sup> Matthew Croad,<sup>1</sup> Yulia Rogan,<sup>1</sup> Johannes C. Jansen,<sup>2</sup> Paola Bernardo,<sup>2</sup> Fabio Bazzarelli,<sup>2</sup> Neil B. McKeown<sup>1\*</sup>

Microporous polymers of extreme rigidity are required for gas-separation membranes that combine high permeability with selectivity. We report a shape-persistent ladder polymer consisting of benzene rings fused together by inflexible bridged bicyclic units. The polymer's contorted shape ensures both microporosity—with an internal surface area greater than 1000 square meters per gram—and solubility so that it is readily cast from solution into robust films. These films demonstrate exceptional performance as molecular sieves with high gas permeabilities and good selectivities for smaller gas molecules, such as hydrogen and oxygen, over larger molecules, such as nitrogen and methane. Hence, this polymer has excellent potential for making membranes suitable for large-scale gas separations of commercial and environmental relevance.

Commercially important membrane-based gas separations include O<sub>2</sub> and N<sub>2</sub> enrichment of air, hydrogen recovery from ammonia production or hydrocarbon processing, and the upgrading of natural gas (1). They also have potential for both post-combustion and pre-combustion CO<sub>2</sub> capture during electricity generation from fossil fuels (2, 3). Polymer mem-

branes provide an energy-efficient method for gas separations because they do not require thermal regeneration, a phase change, or active moving parts in their operation and as such are predicted to play a growing role in an energy-constrained and low-carbon future (4). However, polymers suffer from a well-defined trade-off between the desirable properties of permeability and selec-

tivity for the required gas component. Presently, most commercial gas-separation membranes are based on a few polymers with low permeability and high selectivity; therefore, large membrane areas are required to compensate for lack of permeance, which increases costs and space requirements for large-scale applications. Unfortunately, highly permeable microporous polymers demonstrate insufficient selectivity for practical applications because, unlike classical molecular sieves such as zeolites, they possess ill-defined voids that because of chain flexibility fluctuate in size and so have limited size-selectivity (5). However, microporous polymers have the great advantage over classical inorganic molecular sieve materials of being easily processed into membranes (such as thin coatings or hollow fibers). Therefore, it is an important challenge to develop microporous polymers that behave as efficient

<sup>1</sup>School of Chemistry, Cardiff University, Cardiff CF10 3AT, UK.

<sup>2</sup>Institute on Membrane Technology, Consiglio Nazionale delle Ricerche, ITM-CNR, c/o University of Calabria, Via P. Bucci 17/C, 87030 Rende (CS), Italy.

\*To whom correspondence should be addressed. E-mail: [mckeownnb@cardiff.ac.uk](mailto:mckeownnb@cardiff.ac.uk).